

pubs.acs.org/crystal Article

Remarkable Similarity of Molecular Packing in Crystals of Racemic and Enantiopure 2-Phenylpropionamide: Z'=4 Structures, Molecular Disorder, and the Formation of a Partial Solid Solution

Raúl Castañeda, Sergei V. Lindeman, Arcadius V. Krivoshein,* Alejandro J. Metta-Magaña, Yongli Chen, and Tatiana V. Timofeeva*



Cite This: Cryst. Growth Des. 2022, 22, 4592–4600



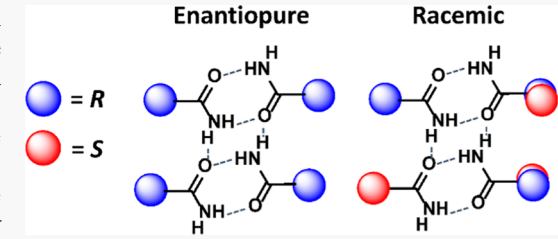
ACCESS I

Metrics & More

Article Recommendations

Supporting Information

ABSTRACT: Substituted acetamides (many of which are chiral) are known to be pharmacologically active. 2-Phenylpropionamide (2PPA) is one of the simplest chiral α -substituted acetamides and thus is of interest as a model compound in the growth and design of pharmaceutical crystals. In this study, the crystal structures of racemic and enantiopure forms of 2PPA were determined for the first time using single-crystal X-ray diffraction at 100 K. The relationship between the signs of optical rotation and the absolute configurations is (+)-(S)-2PPA and (-)-(R)-2PPA. Four symmetrically independent molecules with different conformations are observed in crystals



of both racemic and enantiopure forms. Remarkably, all forms adopt very similar supramolecular structures, H-bonded corrugated layers, that can be described using a $R_2^2(8)R_6^4(16)$ graph set. The outer surfaces of these layers are built of nonpolar phenyl groups, and their inner structures are composed of H-bonded amide groups. The presence of these layers determines the thin plate shape of 2PPA crystals. Spectroscopically, the racemic and enantiopure forms substantially differ only in the low-frequency Raman region. X-ray diffraction data suggest that the racemic form of 2PPA is a partial solid solution made possible by statistical occupancy of molecular positions by (R)- and (S)-enantiomers.

■ INTRODUCTION

 α -Substituted acetamides exhibit a broad range of pharmacological effects, such as antiepileptic, anticancer, and antiviral activities. Since many pharmaceuticals (e.g., antiepileptic drugs) are orally administered, their supramolecular structure in the crystalline state relates to aqueous solubility, polymorph control during manufacturing, and stability upon storage. Thus, a predictive understanding of the crystal structure is of value in the rational design of novel drug leads and in formulation development.

Crystal structures of several α -substituted acetamides have been determined previously. $^{4-10}$ In our survey of the Cambridge Structural Database (CSD, ver. 5.42, November 2020 release; Groom et al. 11), we found only a handful of structures for chiral substituted acetamides. For 3-methyl-2-phenylbutyramide, both racemic and enantiopure forms have been studied (LIDCOT, LIDCUZ, LIDDAG, and LIDDAG01). It was observed that the crystals of this compound are built of ribbon synthons that can be described by a $R_2^2(8)$ $R_4^2(8)$ graph set. For 2-(4-t-butylphenyl)propionamide, only the racemic form has been studied (ZEPGAF), and a $R_2^2(8)$ $R_6^4(16)$ layer synthon was observed. 12

In one of our previous studies, ⁸ we solved crystal structures of racemic and enantiopure forms of 2-phenylbutyramide (VOQGUF, VOQHAM, and VOQHEQ) and unambiguously assigned the absolute configurations of its enantiomers. 2-

Phenylbutyramide is a promising experimental anticonvulsant³ that can be regarded as a fragment of the well-known antiepileptic drug phenobarbital (Scheme 1). Despite different molecular conformations, racemic and enantiopure forms of that compound adopt very similar crystal structures built of $R_2^2(8)R_4^2(8)$ ribbon synthons (this similarity is in part due to the existence of two conformers in the enantiopure forms). For the racemic form of 2PBA, a second polymorphic modification with a C(7) chain synthon was described.¹³

The title compound of this study, 2-phenylpropionamide (2PPA; also known as hydratropamide, Scheme 1), is a lower homolog of 2-phenylbutyramide and thus one of the simplest possible α -aryl- α -alkyl-substituted acetamides (it was first reported in 1889¹⁴). This simplicity makes it an interesting structural model for this class of compounds. Like 2-phenylbutyramide, 2PPA exhibits pharmacological activity. ¹⁵

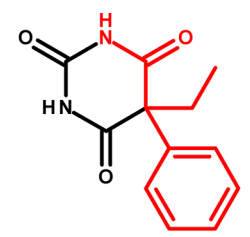
Here, we report the crystal structures of racemic and enantiopure forms of 2PPA and discuss the reasons why these

Received: May 3, 2022 Revised: June 9, 2022 Published: June 27, 2022



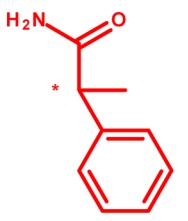


Scheme 1. Structures of Phenobarbital, 2-Phenylbutyramide, and 2-Phenylpropionamide^a



5-ethyl-5-phenylpyrimidine-2,4,6-trione (phenobarbital)

2-phenylbutyramide



2-phenylpropionamide (2PPA)

^aThe chiral carbon is marked with an asterisk.

Table 1. Crystallographic and Structure Refinement Data for 2PPA (C₉H₁₁NO, FW 149.19)

parameter	rac-2PPA	(R)-2PPA	(S)-2PPA
melting point (°C)	95.7(2)	101.5(2)	101.8(1)
crystal size, mm	$0.5 \times 0.15 \times 0.05$	$0.5 \times 0.4 \times 0.1$	$0.4 \times 0.35 \times 0.045$
<i>T,</i> K	100	100	100
radiation type	Mo Kα (0.71073 Å)	Cu Kα(1.54184 Å)	Cu Kα (1.54184 Å)
absorption correction	multi-scan (SADABS, Bruker)	Gaussian (SCALE3 ABSPACK, Oxford)	Gaussian (SCALE3 ABSPACK, Oxford)
crystal system, space group	monoclinic, Ia	monoclinic, P2 ₁	monoclinic, P2 ₁
a, Å	9.9350(4)	9.7640(1)	9.7728(2)
b, Å	11.8216(6)	6.09218(8)	6.0917(1)
c, Å	28.806(2)	28.0229(3)	28.0402(5)
α , deg	90.00	90.00	90.00
β , deg	99.239(5)	99.987(1)	99.991(2)
γ, deg	90.00	90.00	90.00
V, Å ³	3339.3(3)	1641.66(3)	1644.01(5)
<i>Z</i> , Z'	16, 4	8, 4	8, 4
$ ho_{ m cal}$ g/cm ³	1.197	1.207	1.205
μ , mm ⁻¹	0.078	0.630	0.629
2Θ range for data collection, deg	5.4 to 47.7	9.1 to 141.1	9.1 to 141.0
reflections collected	34575	29313	29847
independent reflections	6074	6078	6227
$R_{\rm int}$	0.0463	0.0293	0.0484
resolution, Å	0.83	0.82	0.82
goodness-of-fit on F^2	1.081	1.101	1.054
$R\left[F^2 \ge 2\sigma(F^2)\right]$	0.0587	0.0334	0.0472
$wR(F^2)$	0.1428	0.0832	0.1322
largest diff. peak/hole, e Å ⁻³	0.22/-0.17	0.18/-0.17	0.29/-0.21
Flack x parameter	not appl.	-0.08(22)	0.12(35)
Hooft y parameter	not appl.	-0.04(5)	0.17(7)
Parsons z parameter	not appl.	-0.03(8)	0.14(10)
no. of Bijvoet pairs	not appl.	3486 (93.6%)	5046 (99.7%)

structures are remarkably similar. Additionally, using anomalous dispersion of X-rays, we confirmed the relation between the signs of optical rotation and the absolute configurations of 2PPA enantiomers.

■ EXPERIMENTAL SECTION

Chemicals. Enantiopure and racemic forms of 2PPA were purchased from Enamine Ltd. (Monmouth Junction, NJ) and used without further purification. Analysis of the enantiomers using chiral high performance liquid chromotagraphy (HPLC) indicates essentially 100% enantiomeric excess (Figure S1). HPLC-grade hexanes, acetone, methanol, and acetonitrile were purchased from MilliporeSigma (Burlington, MA).

Chiral HPLC. All separations were conducted on a Chiralcel OD-RH column (150 \times 4.6 mm, 5 μ m particle size; Chiral Technologies, West Chester, PA) at 20 °C on a 1260 Infinity HPLC system (Agilent Technologies, Santa Clara, CA) consisting of a G1379B micro

degasser, a G1312B binary pump, a G1329B standard autosampler, a G1316A thermostatted column compartment, and a G1315C diode array UV—Vis detector with a 2 μ L, 3 mm pathlength micro flow cell. The detection wavelength was 258 nm, and the flow rate was set to 0.3 mL/min. Acetonitrile was used as the mobile phase. The injected 50 μ L samples were 2 mM solutions of enantiopure forms of 2PPA in the mobile phase.

Crystal Growth. Crystals of enantiopure and racemic forms of 2PPA were grown by slow evaporation from 9 mL of 15 mg/mL solution in hexanes/acetone (2:1, vol/vol) in glass vials (liquid scintillation vials, 20 mL capacity) at room temperature in a desiccator (the solvent was allowed to evaporate completely). Crystallization of all three forms yielded very similar thin colorless plates.

In order to prepare the samples for the binary melting point diagram, solid (R)-2PPA and (S)-2PPA were mixed in the appropriate proportions, dissolved in hexanes/acetone (2:1, vol/vol), and

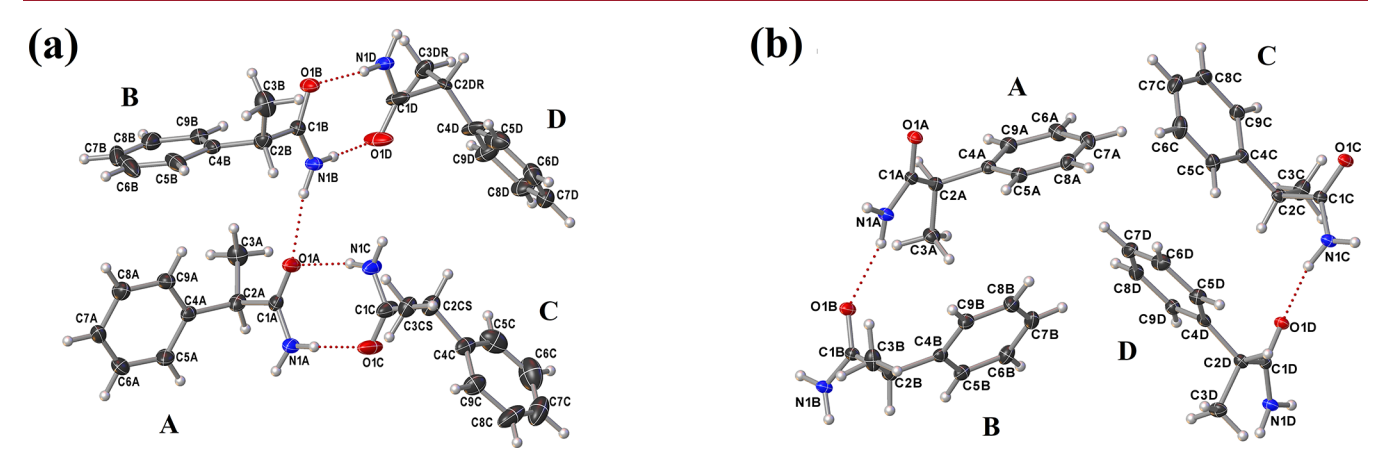


Figure 1. Molecular structures with atomic numbering schemes of four independent molecules (A–D) in crystals of the racemate (panel a) and the (R)-enantiomer (panel b).

crystallized as above, except that 6.6 mL of 15 mg/mL solution was used for each sample.

Single-Crystal X-ray Diffraction Analysis. For the enantiopure forms, X-ray diffraction data were collected at 100 K on an Oxford SuperNova Atlas CCD diffractometer (Rigaku Oxford Diffraction, The Woodlands, TX) using Cu K α radiation (λ = 1.54184 Å). The data were corrected for absorption in the CrysAlis^{PRO} program (ver. 1.171.39.46, Rigaku Oxford Diffraction, The Woodlands, TX) using a combined approach incorporating numerical absorption correction based on Gaussian integration over a multifaceted crystal model as well as an empirical absorption correction using spherical harmonics as implemented in the SCALE3 ABSPACK scaling algorithm.

Preliminary data for the enantiopure forms were collected on a D8 Venture diffractometer with a PHOTON II CPAD detector (Bruker AXS, Madison, WI) using Cu K α radiation ($\lambda = 1.54184$ Å).

For the racemic form, \tilde{X} -ray diffraction data were collected at 100 K on a SMART APEX II CCD diffractometer (Bruker AXS, Madison, WI) using graphite-monochromatized Mo K α radiation (λ = 0.71073 Å) and corrected for absorbance using a multi-scan approach in the SADABS program as implemented in the APEX3 crystallography software suite (Bruker AXS, Madison, WI).

Structures were solved with SHELXT and refined with SHELXL using a full-matrix least-squares minimization. ¹⁶ The positions of hydrogen atoms at the α -carbon and aromatic carbons were refined using the riding model, while the positions of hydrogen atoms in the CH $_3$ group were refined by considering this group as an idealized rotating group. Fixed $U_{\rm iso}$ values of 1.2 times were used for all CH and CH $_3$ groups. The hydrogen atoms involved in hydrogen bonding were located in the difference maps and refined with individual isotropic displacement parameters. SADI restraint with a 0.02 e.s.d. was used to link all nitrogen-hydrogen distances in the (R)- and (S)-enantiomers. DFIX restraint with 0.90 distance and 0.02 e.s.d. was applied to all nitrogen-hydrogen distances in the racemate.

Crystals of the racemic form of 2PPA have two molecular positions filled by molecules of specific chirality (R or S) and two other molecular positions, where molecules of different chirality are interchangeable. Such a structure is known as a "partial solid solution". During structure refinement, the chiral center was refined as disordered with the phenyl rings and amide groups in fixed positions and full occupancy. To obtain a stable refinement, the occupancy of molecule C was fixed to 0.5 for each enantiomer (it is worth mentioning that for this molecule, refining the occupancy led to values close to 0.5). For molecule D, the occupancy of the (S)-enantiomer was freely refined with the occupancy of the (S)-enantiomer. The resulting occupancies for this disordered position were 0.67 for the (S)-enantiomer and 0.33 for the (S)-enantiomer.

Crystals of 2PPA have a strong tendency toward twinning. Luckily, twinning was negligible in the crystals of the (R)-enantiomer. In the case of the (S)-enantiomer (7.0% twinning), a twin matrix was

obtained using the Olex2 program (ver. 1.3, OlexSys Ltd, Durham, UK¹⁷); this twin matrix was used during refinement. The strongest (12.3%) twinning was observed in the crystals of the racemic form (this was true for several batches of the crystals). Our attempt to use a twin matrix failed. The best quality structure of the racemic form was obtained when no twin processing was applied.

The absolute configuration of the enantiomers was determined based on anomalous dispersion intensities described by the Flack x parameter, ¹⁸ the Hooft y parameter, ¹⁹ and the Parsons z parameter.

Face indexing of representative crystals was carried out on a SMART APEX II CCD diffractometer (Bruker AXS, Madison, WI) using graphite-monochromatized Mo $K\alpha$ radiation (λ = 0.71073 Å). Miller indices of various faces were calculated using the Index Crystal Faces plug-in of the APEX3 crystallography software suite.

Details of crystal structures, data collection, and structure refinement are given in Table 1.

The atomic coordinates have been deposited with the Cambridge Crystallographic Data Center: CCDC 2165460 entry for *rac-*2PPA, CCDC 2165461 entry for (-)-(R)-2PPA, and CCDC 2165462 entry for (+)-(S)-2PPA. These data can be obtained free of charge from the Director, CCDC, 12 Union Road, Cambridge CB2 1EZ, UK (fax: +44 1223 336033; e-mail: deposit@ccdc.cam.ac.uk; website: www.ccdc.cam.ac.uk).

Polarimetry. Optical rotation of 5 g/100 mL solutions of the compounds under investigation in methanol was measured at the sodium D-line wavelength (589 nm) in a 100 mm optical cell on an Autopol III polarimeter (Rudolph Research Analytical, Hackettstown, NJ) at room temperature (22–24 °C). The observed optical rotation values were converted to specific optical rotation, $[\alpha]_D$, using the formula: $[\alpha]_D = \alpha \times 100/l \times c$, where α is the observed optical rotation (degrees), l is the pathlength (decimeters), and c is the concentration (g/100 mL).

Melting Point Determination. Melting curves of finely ground crystals were recorded on an OptiMelt MPA100 automated melting point system with digital image processing technology controlled by MeltView ver. 1.107 software (Stanford Research Systems, Sunnyvale, CA). A heating rate of 1 °C/min was used. The clear point was defined as the 10% threshold.

Vibrational Spectroscopy. Infrared (IR) spectra of finely ground crystals were recorded at room temperature (22–24 °C) on a Nicolet iS5 FT-IR spectrometer fitted with an iD7 single-bounce monolithic diamond attenuated total reflectance (ATR) accessory and controlled by OMNIC ver. 9.8.372 software (Thermo Fisher Scientific, Madison, WI). The spectral range was 4000–525 cm⁻¹, and the resolution was set at 4 cm⁻¹. Thirty-two spectra were collected and averaged for each sample or background measurement. Other acquisition settings were as follows: 2 levels of zero filling, Happ-Genzel apodization, and Mertz phase correction. A two-segment (4000–2000 and 2000–525 cm⁻¹) linear Baseline Correction and an Advanced ATR Correction were applied.

Crystal Growth & Design pubs.acs.org/crystal Article

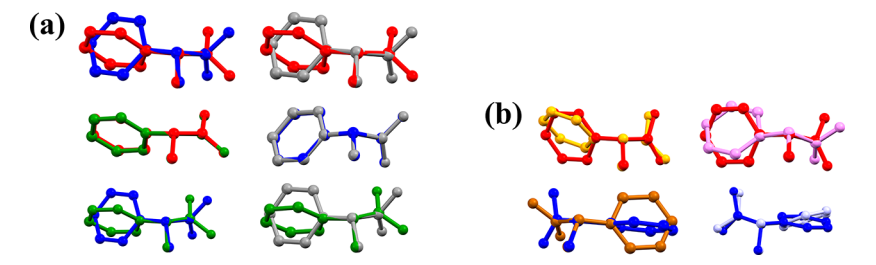


Figure 2. Overlay visualization of the four symmetrically independent molecules (A through D) in crystals of the (R)-enantiomer (panel a) and the racemate (panel b). Different molecules had been drawn in different colors. For panel (a), the colors are red for A, blue for B, gray for C, and green for D. For panel (b), the colors are red for (R)-A, yellow for (R)-C, blue for (S)-B, orange for (S)-C, magenta for (R)-D, and cyan for (S)-D.

Table 2. Dihedral Angles Reflecting the Conformational Differences between Symmetrically Independent Molecules in the Racemic and Enantiopure Forms

dihedral angle (deg)	molecule A	molecule B	molecule C	molecule D					
(R)-2PPA									
C1-C2-C4 to C9-C4-C5	36.0(2)	68.5(2)	70.2(2)	36.6(2)					
C1-C2-C4 to N1-C1-O1	48.8(2)	55.4(2)	54.2(2)	46.6(2)					
(S)-2PPA									
C1-C2-C4 to C9-C4-C5	36.1(3)	68.3(3)	69.8(3)	36.3(3)					
C1-C2-C4 to N1-C1-O1	48.8(3)	54.8(3)	54.6(3)	46.7(3)					
rac -2PPA a									
C1-C2-C4 to C9-C4-C5	69.4(3)	5.6(4)	(R): 36.8(7)	(R): 74.1(5)					
			(S): 74.1(7)	(S): 72.4(4)					
C1-C2-C4 to N1-C1-O1	76.6(3)	81.9(3)	(R): 75(1)	(R): 29.2(6)					
			(S): 34.4(6)	(S): 32.4(5)					

^aIn the racemic form, two crystallographic positions (C and D) can be occupied by either the (R)-enantiomer or the (S)-enantiomer.

Raman spectra of finely ground crystals were recorded at room temperature (22–24 °C) on a DXR2 or DXR3 SmartRaman spectrometer fitted with a 180° sampling accessory and a 785 nm HP laser and controlled by OMNIC for Dispersive Raman ver. 9.9.535 software (Thermo Fisher Scientific, Madison, WI). The spectral range was 3382–50 cm $^{-1}$, and the estimated resolution was 2.4–4.3 cm $^{-1}$ (25 $\mu{\rm m}$ slit aperture). 20 mW laser power and 3 s exposure time were used. Ten spectra were collected and averaged for each sample measurement, and twenty spectra were collected and averaged for each background measurement. A second-order polynomial fluorescence correction was applied.

RESULTS AND DISCUSSION

Molecular Structure and Stereochemistry. Racemic and enantiopure forms of 2PPA were crystallized from hexanes/acetone (2:1, vol/vol). Crystal structures were solved using single-crystal X-ray diffraction at 100 K (Table 1). In all three forms of 2PPA, crystals are built of four symmetrically independent molecules (A, B, C, and D; Figure 1). In general, Z' = 4 structures are rather uncommon. However, the amide—amide cyclic dimer synthon found in 2PPA (see below) seems to impart a high tendency toward Z' > 1 structures.²¹

Absolute configurations of 2PPA enantiomers were inferred from intensities of anomalous dispersion of X-rays by N and O atoms measured using a high-intensity Cu K α source. Independent determinations were carried out for (R)- and (S)-enantiomers. Even though the 2PPA molecule consists of only "light" atoms, we were able to achieve 94–100% coverage of theoretically possible Bijvoet pairs (Table 1) and reliably assign the absolute configurations (indeed, the Flack x, Hooft y, and Parsons z values are in excellent agreement with each other). The optical rotation of solutions of enantiopure forms of 2PPA in methanol was measured by polarimetry at 589 nm. For (S)-2PPA, $\alpha_{[D]}$ is +36.72 \pm 0.06 deg·mL·g⁻¹·dm⁻¹ (M \pm

SD, n = 5). For (R)-2PPA, $\alpha_{[D]}$ is -41.01 ± 0.01 deg·mL·g⁻¹· dm⁻¹ (M \pm SD, n = 7). These values are in accordance with the literature, such as the study by Pettersson²² (Table S1; note that the magnitude of optical rotation depends on solvent polarity). Thus, the relationship between the signs of optical rotation and the absolute configurations can be confirmed as (+)-(S)-2PPA and (-)-(R)-2PPA.

Since the crystal structures of the (S)- and (R)-enantiomers are identical, in our subsequent discussion we will use only the data for the (R)-enantiomer. Bond lengths and bond angles in the molecules are in the range of the typical values for organic compounds. However, a great deal of diversity is observed in molecular conformations (specifically, in the orientation of the phenyl group relative to the plane of the three-carbon fragment containing the chiral α -carbon). These differences can be readily observed in an overlay of the four conformers of the (R)-enantiomer (Figure 2); dihedral angles for all forms are given in Table 2. For enantiopure crystals, the molecular conformations are similar within pairs A-D and B-C but different between these two pairs. It should be mentioned that an attempt to find a model with a smaller number of symmetrically independent molecules was unsuccessful. Table 2 shows that the molecular conformations are more variable in the racemic form compared to the enantiopure form. Notably, the range of phenyl group orientations in 2PPA molecules is much broader than in the molecules of its higher homolog, 2phenylbutyramide.⁸ This could be due to the smaller steric bulk of the methyl substituent versus the ethyl substituent at the chiral α carbon. Some of these variations in the phenyl group orientations are due to molecular positions C and D being able to statistically accommodate molecules of opposite chirality—in other words, the same molecular position can be occupied by either the (R)-enantiomer or the (S)-enantiomer.

Crystal Growth & Design pubs.acs.org/crystal Article

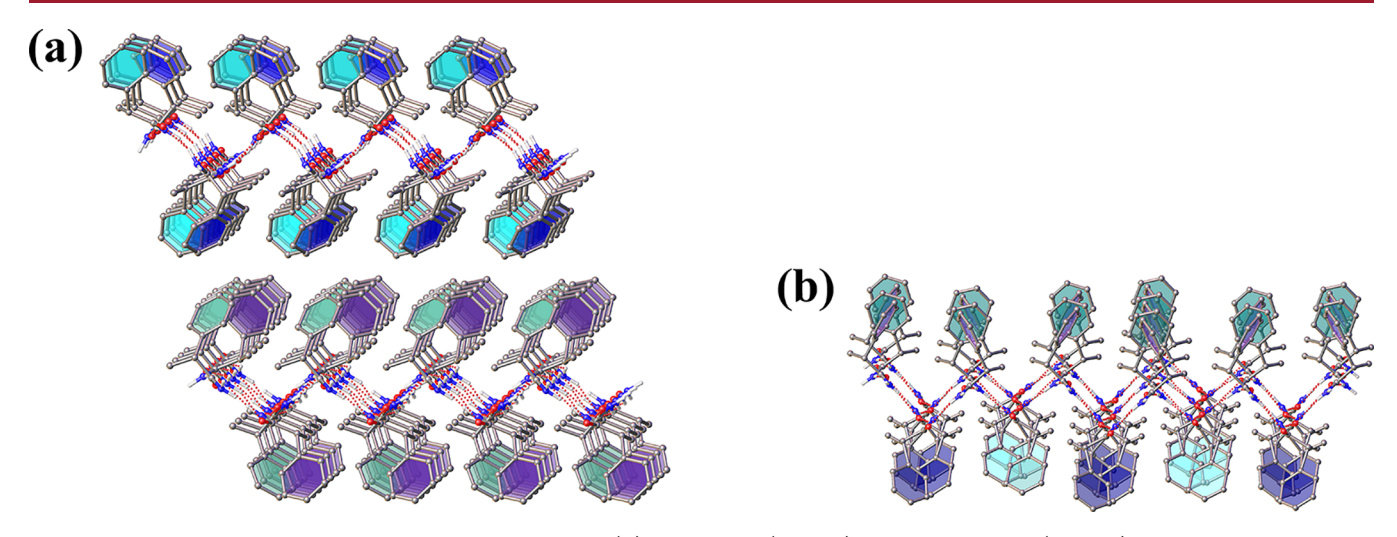


Figure 3. Packing of individual 2D layers in crystals of the (R)-enantiomer (panel a) and the racemate (panel b). For both structures, the projection along the a axis is shown. The phenyl rings have been highlighted in different colors to indicate different symmetrically independent molecules.

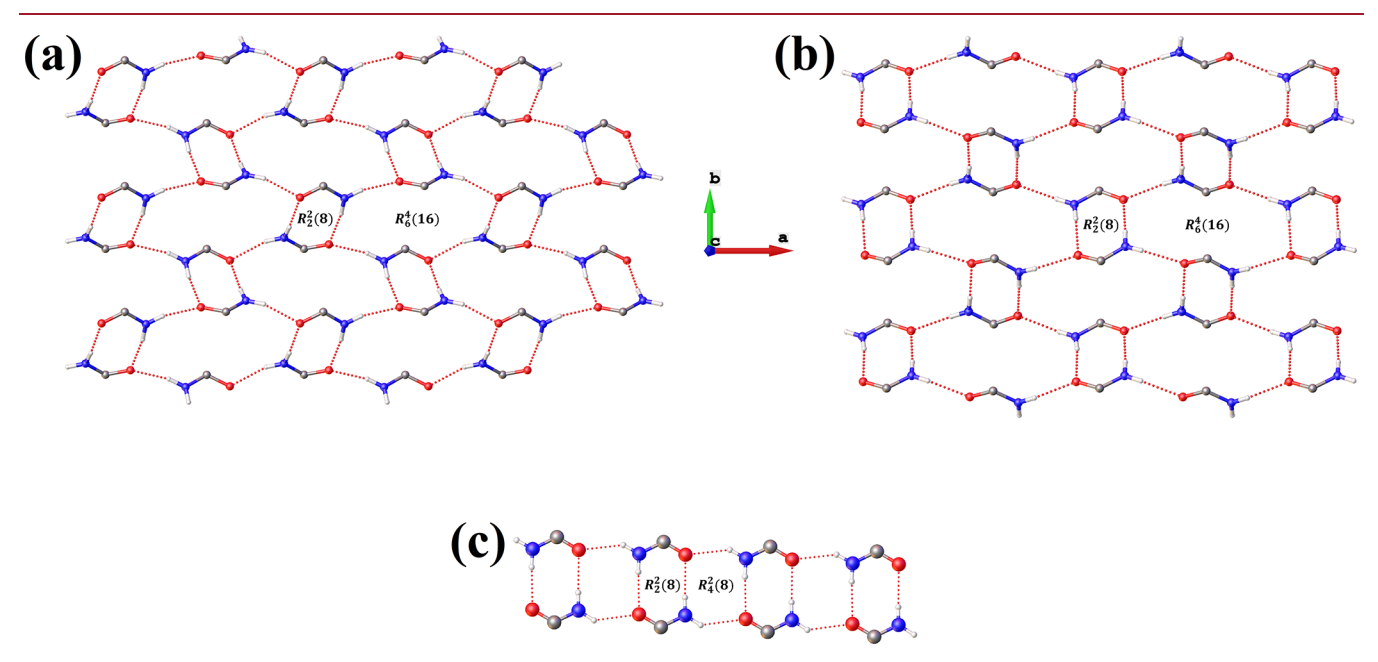


Figure 4. H-bond patterns in crystals of the (R)-enantiomer (panel a) and the racemate (panel b); phenyl and methyl substituents are omitted for clarity. Hydrogen bonds are drawn as dashed red lines. For the (R)-enantiomer, the H-bond pattern of the second independent layer is not shown as it is very similar to the first layer. For comparison, panel c illustrates a one-dimensional H-bonded ribbon, which is the most common supramolecular synthon in substituted acetamides.

A similar situation was recently described by Lodochnikova and Fayzullin with collaborators²³ for a racemic 1,5-dihydro-2H-pyrrol-2-one derivative that forms a partial solid solution. In the polymorphic modification with Z'=4, two out of four symmetrically independent molecules are disordered.

Supramolecular Structure. The molecular packing in racemic and enantiopure crystals is defined by the formation of H-bonded 2D synthons (layers) shown in Figures 3 and 4. The hydrogen bond parameters are given in Table 3.

In racemic crystals, parallel layers are formed by four independent molecules A–D. Considering that molecules C and D are disordered in such way that same molecular positions are taken by molecules of different chirality, one can say that effectively there are six independent molecules. As we mentioned above, such a situation can be defined as a partial

solid solution of enantiomorphs.^{24–26} Petit with collaborators²⁶ mention isosterism and preservation of the strongest intermolecular interactions upon substitution as the two structural requirements for the existence of enantiomeric solid solutions. In such conditions, opposite enantiomers with similar molecular shapes can participate in the same H-bonded synthons. Conformational flexibility also allows for molecular mimicry and the same relative positions of different enantiomers in the crystal structure.

Binary phase diagrams for melting can be used to distinguish between racemic compounds, racemic mixtures, and solid solutions (pseudoracemates). $^{25-27}$ Pettersson 22 constructed a partial diagram (hollow circles and dotted line in Figure 5) for 2PPA samples crystallized from neat acetone. To confirm his results, we prepared 2PPA crystals with a variable ratio of (R)-

Table 3. Hydrogen Bond Geometry in the Racemic and Enantiopure $Forms^k$

D–H···A	D–H distance (Å)	H···A distance (Å)	D–A distance (Å)	D-H-A angle (deg)				
(S)-2PPA								
N1A-H1AA···O1B4 ^a	0.94(2)	2.06(3)	3.000(4)	174(4)				
N1A-H1AB···O1B ^b	0.93(2)	2.06(3)	2.935(4)	156(4)				
N1B-H1BA···O1A ^c	0.92(2)	1.98(3)	2.894(4)	169(5)				
N1B-H1BB···O1A	0.94(2)	1.95(3)	2.873(4)	166(4)				
N1C-H1CA···O1D ^d	0.92(2)	2.00(3)	2.916(4)	173(5)				
N1C-H1CB···O1D ^b	0.92(2)	2.03(4)	2.863(4)	149(5)				
N1D-H1DA···O1C ^e	0.93(2)	2.09(2)	3.017(4)	171(4)				
N1D-H1DB···O1C	0.93(2)	2.05(3)	2.930(4)	157(4)				
(R)-2PPA								
N1A-H1AA···O1B ^f	0.88(2)	2.13(2)	3.002(3)	169(3)				
N1A-H1AB···O1B	0.90(2)	2.08(2)	2.933(2)	159(3)				
N1B-H1BA···O1A ^g	0.90(2)	2.01(2)	2.893(3)	168(3)				
N1B-H1BB···O1A	0.90(2)	2.00(2)	2.868(2)	161(3)				
N1C-H1CA···O1D ^h	0.88(2)	2.04(2)	2.908(2)	166(3)				
N1C-H1CB···O1D	0.91(2)	1.98(2)	2.860(2)	160(3)				
N1D-H1DA···O1C ⁱ	0.91(2)	2.13(2)	3.026(3)	170(3)				
N1D-H1DB···O1C ^g	0.90(2)	2.07(2)	2.923(2)	157(3)				
rac-2PPA								
N1A-H1AA···O1C	0.88(3)	2.09(3)	2.969(5)	178(5)				
N1A-H1AB···O1B ^b	0.88(3)	2.10(3)	2.934(5)	157(4)				
N1B-H1BA···O1D	0.89(3)	2.02(3)	2.908(6)	178(4)				
N1B-H1BB···O1A	0.89(3)	2.04(3)	2.923(5)	171(5)				
N1D-H1DA···O1B	0.90(3)	2.06(3)	2.954(5)	173(6)				
N1D-H1DB···O1D ⁱ	0.88(3)	2.04(3)	2.879(5)	160(5)				
N1C-H1CA···O1A	0.88(3)	2.11(3)	2.986(5)	169(4)				
N1C-H1CB···O1C ^j	0.88(3)	2.07(3)	2.935(5)	167(5)				
aa		1 /0		ha .				

^aSymmetry transformations: 1-x, 1/2+y, -z. ^bSymmetry transformations: -1+x, +y, +z ^cSymmetry transformations: 1-x, -1/2+y, -z. ^dSymmetry transformations: 1-x, 1/2+y, -z. ^eSymmetry transformations: 1-x, -1/2+y, -z. ^fSymmetry transformations: 2-x, -1/2+y, 1-z. ^gSymmetry transformations: 2-x, 1/2+y, 1-z. ^hSymmetry transformations: 1-x, y, z. ⁱSymmetry transformations: 2-x, 1/2+y, 2-z. ^jSymmetry transformations: 1+x, +y, +z. ^kSymmetry transformations: -1/2+x, 2-y, +z; -1/2+x, 1-y, +z.

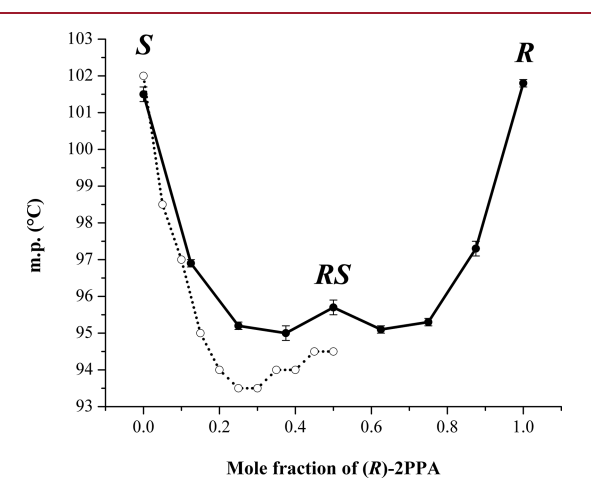


Figure 5. Binary phase diagram for melting (liquidus) of 2PPA crystals with the variable R/S ratio (solid circles and solid line). For comparison, the corresponding data from Pettersson²² are also shown (hollow circles and dotted line).

and (S)-enantiomers using the solvent used in our study (hexanes—acetone mixture) and constructed a full binary phase diagram (solid circles and solid line in Figure 5). Our melting diagram is very similar to that reported by Pettersson.²² The shape of this diagram is inconclusive. The overall shape, with the two eutectic points, suggests a racemic compound. However, the melting point of the racemic form is only slightly higher than the eutectic points. Thus, this diagram also bears some resemblance to the Roozeboom's type III solid solution.^{25,26} Interestingly, Pettersson²² did consider a solid solution as an explanation for the melting diagram of 2PPA. However, based on the limited data (powder X-ray diffraction profiles, IR spectra, and hot-stage microscopy observations) available to him in 1956, he discovered such a possibility. Thus, our study once again illustrates the value of single-crystal X-ray diffraction in structural studies of partial solid solutions. Careful examination of X-ray diffraction peaks and the appropriate adjustments to the refinement procedure (see the Experimental Section) were essential in revealing these structural peculiarities of rac-2PPA crystals. Specifically, the Xray diffraction data allow to rationalize the melting diagram as that of a racemic compound with a partial solid solution formation.

In the crystals of the enantiopure forms, the four independent molecules form antiparallel alternating layers. Figures 3 and 4 demonstrate that despite the above-mentioned differences and differences in space groups and unit cell parameters, H-bonded synthons in racemic and enantiopure crystal structures are very similar. Projections of these layers along axis c demonstrate that these layers have corrugated profiles. All layers are built with alternating 8- and 16-membered H-bonded rings that can be described in terms of graph-set analysis 28 as $R_2^2(8)R_6^4(16)$. The geometric parameters presented in Table 3 demonstrate that H-bonds in 2PPA are of moderate strength. 29

The $R_2^2(8)R_6^4(16)$ synthon is unusual for chiral α -substituted acetamides; such compounds typically form $R_2^2(8)R_4^2(8)$ ribbons (see the Introduction and panel c in Figure 4). The $R_2^2(8)R_6^4(16)$ synthon has previously been observed only in the racemic form of 2-(4-*t*-butylphenyl)propanamide (ZEP-GAF¹²); enantiopure forms of that compound have not been studied yet. In both synthons, H-bonded amide groups form the inner structure, while nonpolar aryl and alkyl groups are on the outer surfaces.

It should be mentioned that both racemic and enantiopure forms of 2PPA crystallize as very thin plates with larger faces developed along the (001) direction (Figure 6). Thus, we can conclude that crystal growth is slow in the direction perpendicular to the most developed (001) faces. The calculated crystal shapes agree with experimental observations (Figure 7); one can see that the most developed faces are parallel to the layers of H-bonded molecules of 2PPA. Recent studies^{30,31} demonstrate the importance of crystal habit in the dissolution rate of pharmaceuticals.

Vibrational Spectra in the Solid State. The main bands in the ATR IR spectra of finely ground crystals of racemic and enantiomeric forms of 2PPA (Figure S2) are as follows: the asymmetric H–N–H stretching band (amide A) at 3348–3357 cm⁻¹, the symmetric H–N–H stretching band (amide B) at 3181–3194 cm⁻¹, and the C=O stretching band (amide I; several components) at 1633–1658 cm⁻¹ (the latter band overlaps with a weaker Amide II band). We previously

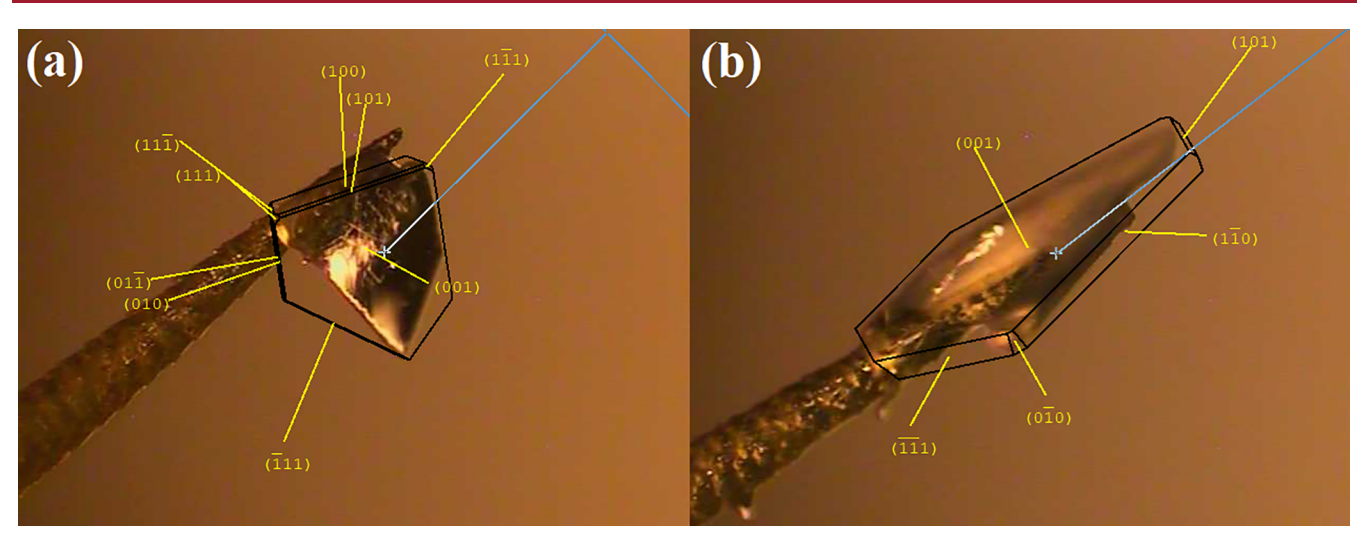


Figure 6. Miller indices in the crystals of the racemate (panel a) and the (R)-enantiomer (panel b).

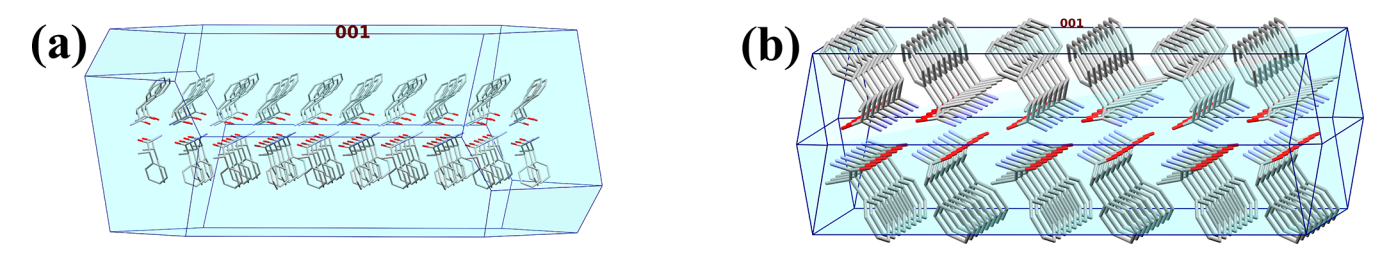


Figure 7. Calculated crystal shapes of the racemate (panel a) and the (R)-enantiomer (panel b).

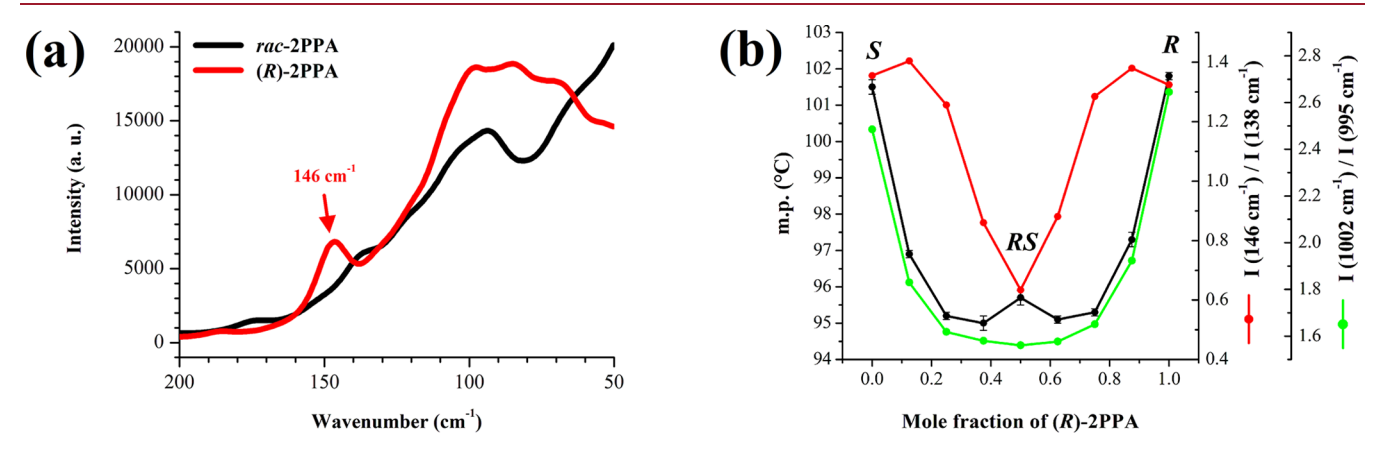


Figure 8. External lattice vibrations in Raman spectra easily distinguish between the crystal structures of racemic and enantiopure forms of 2PPA. Panel (a) shows the low-frequency region of Raman spectra of rac-2PPA and (R)-2PPA (ground crystals). The spectrum of (S)-2PPA (not shown) is identical to that of (R)-2PPA. Panel (b) shows the relative intensities of external (146 cm^{-1}) and internal $(995 \text{ and } 1002 \text{ cm}^{-1})$ vibrations overlaid on the binary melting diagram from Figure 5.

observed very similar spectra for 2-phenylbutyramide^{8,32} and 2,2-diethylacetamide.⁹

The IR spectral differences between the racemic and enantiopure forms are small: (i) minor shifts (9–13 cm⁻¹) in the amide A and amide B frequencies (Figure S2, panel a); (ii) redistribution of the components of amide I band (Figure S2, panel b)—this is reminiscent of what we observed for polymorphs of *rac*-3-phenylpyrrolidine-2,5-dione; ³³ (iii) differences in the fingerprint region (Figure S2, panel c).

Likewise, only small differences between the racemic and enantiopure forms are observed in Raman spectra corresponding to internal vibrational modes (Figure S3). For example, the redistribution of the components of the symmetrical in-plane

ring deformation (ring breathing) band (Figure S3, panel a) may be related to the increased crystallographic disorder in the racemic form (see above). Some of the differences in the fingerprint region of the Raman spectra (such as the increase in the intensity of the 1212 cm⁻¹ band and the emergence of the 1276 cm⁻¹ band in the spectra of the enantiopure forms) are analogous to the corresponding differences in the IR spectra. This similarity of molecular vibrations in solid-state IR and Raman spectra of racemic and enantiopure forms of 2PPA reflects the similarity of H-bonded supramolecular synthons.

However, prominent differences between racemic and enantiopure forms of 2PPA are observed in the low-frequency (<200 cm⁻¹) Raman region corresponding to the external

vibrations of crystalline lattice (Figure 8, panel a). Specifically, the spectra of the enantiopure forms exhibit a new wellresolved peak at 146 cm⁻¹ and a major rearrangement of the overlapped peaks in the 50 to 100 cm⁻¹ region. Can these differences be used to monitor the formation of the "racematetype" crystal structure (partial solid solution) in 2PPA? To answer this question, we recorded Raman spectra of the samples used to construct the binary melting diagram in Figure 5. Panel (b) in Figure 8 shows the relative intensity of the 146 cm⁻¹ peak overlaid on the melting diagram. For comparison, the ratio of the component intensities corresponding to the phenyl ring breathing vibration is plotted also. It is interesting to note that the intensity of the 146 cm⁻¹ external vibration first stays about the same but then decreases sharply in the vicinity of the 1:1 ratio of the enantiomers. Thus, this peak may be indicative of the formation of a partial solid solution. At the same time, the change in the ring breathing internal vibrations (1002 and 995 cm⁻¹) occurs gradually and generally coincides with the melting point depression. Our observations on the utility of the low-frequency region of Raman spectra in monitoring subtle differences in crystal structures are in line with the previous literature reports. 34,35

CONCLUSIONS

In this study, we examined structural features of one of the simplest possible α -aryl- α -alkyl-substituted acetamides, 2PPA. Both racemic and enantiopure forms of this compound were examined. Based on anomalous dispersion of X-rays and polarimetry, the relationship between the signs of optical rotation and the absolute configurations was confirmed as (+)-(S)-2PPA and (-)-(R)-2PPA.

We found that molecular conformational flexibility and similar shapes of (R)- and (S)-enantiomers of 2PPA allow the formation of very similar molecular H-bonded 2D synthons (layers) in crystals of the racemic and enantiopure forms. The observed planar shape of 2PPA crystals is consistent with such layers, where the inner layer structure is enforced by H-bonded amide groups and the nonpolar aryl and alkyl groups are located on the outer surfaces. This remarkable similarity of supramolecular synthons and packing in 2PPA crystals can be rationalized as follows. (R)- and (S)-enantiomers of a given molecule strive to form similar molecular synthons. In this situation, multiple molecular conformations are beneficial in achieving the closest possible packing and high-Z' structures favored.

In general, the similarity of crystal structures of racemic and enantiopure forms of 2PPA is reflected in the very similar solid-state vibrational (IR and Raman) spectra. At the same time, lattice vibrational modes (observed in the low-frequency region of Raman spectra) are sensitive even to those very small structural differences and can be utilized to monitor the formation of the "racemate-type" crystal structure (partial solid solution) in 2PPA.

The knowledge of the solid-state structure of this simple α -substituted acetamide, 2PPA, is expected to assist in rational control of the solubility and stability of chiral solid pharmaceuticals containing the α -substituted amide group pharmacophore.

ASSOCIATED CONTENT

Supporting Information

The Supporting Information is available free of charge at https://pubs.acs.org/doi/10.1021/acs.cgd.2c00509.

Summary of polarimetry data, chiral HPLC chromatograms, IR spectra, and Raman spectra (PDF)

Accession Codes

CCDC 2165460–2165462 contain the supplementary crystallographic data for this paper. These data can be obtained free of charge via www.ccdc.cam.ac.uk/data_request/cif, or by emailing data_request@ccdc.cam.ac.uk, or by contacting The Cambridge Crystallographic Data Centre, 12 Union Road, Cambridge CB2 1EZ, UK; fax: +44 1223 336033.

AUTHOR INFORMATION

Corresponding Authors

Arcadius V. Krivoshein — Department of Chemistry, New Mexico Highlands University, Las Vegas, New Mexico 87701, United States; orcid.org/0000-0002-5213-7303; Phone: (203) 942-7214; Email: akrivoshein@hotmail.com Tatiana V. Timofeeva — Department of Chemistry, New Mexico Highlands University, Las Vegas, New Mexico 87701, United States; orcid.org/0000-0001-7475-3206; Phone: (505) 454-3362; Email: tvtimofeeva@nmhu.edu

Authors

Raúl Castañeda — Department of Chemistry, New Mexico Highlands University, Las Vegas, New Mexico 87701, United States

Sergei V. Lindeman — Department of Chemistry, Marquette University, Milwaukee, Wisconsin 53233, United States Alejandro J. Metta-Magaña — Department of Chemistry and Biochemistry, The University of Texas at El Paso, El Paso, Texas 79968, United States; ocid.org/0000-0001-9993-

Yongli Chen – Department of Natural Science, Hawaii Pacific University, Honolulu, Hawaii 96813, United States

Complete contact information is available at: https://pubs.acs.org/10.1021/acs.cgd.2c00509

Notes

The authors declare no competing financial interest.

ACKNOWLEDGMENTS

We thank Drs Mohammed Ibrahim (Thermo Fisher Scientific, San Jose, CA), Vladimir V. Ermolenkov (The University at Albany-SUNY, Albany, NY), and Laurie E. McNeil (The University of North Carolina at Chapel Hill, Chapel Hill, NC) for helpful discussions of Raman spectroscopy. This study was supported in part by grants from the National Science Foundation's PREM program (award nos. DMR-1523611 and DMR-2122108; to T.V.T.), New Mexico INBRE (Institutional Development Award from the National Institute of General Medical Sciences of the National Institutes of Health, award no. P20GM103451; to A.V.K.), and New Mexico EPSCoR (award no. OIA-1757207; to T.V.T., A.V.K., and R. C.). The Bruker D8 Venture diffractometer at the University of Texas at El Paso was acquired using funds from the National Science Foundation's MRI program (award no. CHE-18278750).

■ REFERENCES

(1) Gleave, M. E.; Sato, N.; Sadar, M.; Yago, V.; Bruchovsky, N.; Sullivan, L. Butyrate analogue, isobutyramide, inhibits tumor growth and time to androgen-independent progression in the human prostate LNCaP tumor model. *J. Cell. Biochem.* **1998**, *69*, 271–281.

- (2) Qiu, J.; Gong, Q.; Gao, J.; Chen, W.; Zhang, Y.; Gu, X.; Tang, D. Design, synthesis and evaluation of novel phenyl propionamide derivatives as non-nucleoside hepatitis B virus inhibitors. *Eur. J. Med. Chem.* **2018**, *144*, 424–434.
- (3) Krivoshein, A. V. α-Substituted lactams and acetamides: Ion channel modulators that show promise in treating drug-resistant epilepsy. *Cent. Nerv. Syst. Agents Med. Chem.* **2020**, 20, 79–87.
- (4) Cohen-Addad, C.; Grand, A. Structures cristallines de derives des acides dipropylacétique et tripropylacétique. II. N-Propyl dipropylacétamide et dibutylacétamide. Acta Crystallogr., Sect. B: Struct. Crystallogr. Cryst. Chem. 1974, 30, 1342–1346.
- (5) Wang, J.; Li, H.; Sun, H. 2-(4-Bromophenyl)-2-methylpropanamide. Acta Crystallogr., Sect. E: Struct. Rep. Online 2010, 66, o925.
- (6) Jasinski, J. P.; Golen, J. A.; Siddegowda, M. S.; Yathirajan, H. S.; Swamy, M. T. 2,2-Diphenylacetamide. *Acta Crystallogr., Sect. E: Struct. Rep. Online* **2011**, *67*, o1992–o1993.
- (7) Nichol, G. S.; Clegg, W. 1-(2-Cyclohex-2-enylpropyonyl)-3-methylurea, 2-ethyl-5-methylhexanamide and 2-ethylpentanamide: Three products of barbiturate decomposition. *Acta Crystallogr., Sect. C: Cryst. Struct. Commun.* **2011**, *67*, o13–o17.
- (8) Khrustalev, V. N.; Sandhu, B.; Bentum, S.; Fonari, A.; Krivoshein, A. V.; Timofeeva, T. V. Absolute configuration and polymorphism of 2-phenylbutyramide and α -methyl- α -phenylsuccinimide. *Cryst. Growth Des.* **2014**, *14*, 3360–3369.
- (9) Krivoshein, A. V.; Ordonez, C.; Khrustalev, V. N.; Timofeeva, T. V. Distinct molecular structures and hydrogen bond patterns of α , α -diethyl-substituted cyclic imide, lactam, and acetamide derivatives in the crystalline phase. *J. Mol. Struct.* **2016**, *1121*, 196–202.
- (10) Khandavilli, U. B. R.; Gavin, D. P.; Maguire, A. R.; Nolan, M.; Lawrence, S. E. Exploring the crystal landscape of 3-methyl-2-phenylbutyramide: Crystallization of metastable racemic forms from the stable conglomerate. *Cryst. Growth Des.* **2018**, *18*, 3549–3557.
- (11) Groom, C. R.; Bruno, I. J.; Lightfoot, M. P.; Ward, S. C. The Cambridge Structural Database. *Acta Crystallogr., Sect. B: Struct. Sci., Cryst. Eng. Mater.* **2016**, 72, 171–179.
- (12) Gao, B.; Zhang, G.; Zhou, X.; Huang, H. Palladium-catalyzed regiodivergent hydroaminocarbonylation of alkenes to primary amides with ammonium chloride. *Chem. Sci.* **2018**, *9*, 380–386.
- (13) Rigin, S.; Armijo, B.; Krivoshein, A. V.; Fonari, M.; Timofeeva, T. Crystal structure and Hirshfeld surface analysis of new polymorph of racemic 2-phenylbutyramide. *Acta Crystallogr., Sect. E: Crystallogr. Commun.* **2019**, *75*, 826–829.
- (14) Janssen, H. Beiträge zur Kenntnifs der Substituirbarkeit der Methylenwasserstoffatome im Benzylcyanid. *Justus Liebigs Ann. Chem.* **1889**, 250, 125–140.
- (15) Chapman, M. V.; Marshall, P. G.; McCrea, P. A.; Sheahan, M. M. Derivatives of acetamide and benzamide as hypnotics. *J. Pharm. Pharmacol.* **1957**, *9*, 20–28.
- (16) Sheldrick, G. M. Crystal structure refinement with SHELX. Acta Crystallogr., Sect. A: Found. Adv. 2015, 71, 3-8.
- (17) Bourhis, L. J.; Dolomanov, O. V.; Gildea, R. J.; Howard, J. A. K.; Puschmann, H. The anatomy of a comprehensive constrained, restrained refinement program for the modern computing environment Olex2 dissected. Acta Crystallogr., Sect. A: Found. Adv. 2015, 71, 59–75.
- (18) Flack, H. D. On enantiomorph-polarity estimation. *Acta Crystallogr., Sect. A: Found. Crystallogr.* **1983**, 39, 876–881.
- (19) Hooft, R. W. W.; Straver, L. H.; Spek, A. L. Determination of absolute structure using Bayesian statistics on Bijvoet differences. *J. Appl. Crystallogr.* **2008**, *41*, 96–103.
- (20) Parsons, S.; Flack, H. D.; Wagner, T. Use of intensity quotients and differences in absolute structure refinement. *Acta Crystallogr., Sect. B: Struct. Sci., Cryst. Eng. Mater.* **2013**, *69*, 249–259.
- (21) Steed, K. M.; Steed, J. W. Packing problems: High Z' crystal structures and their relationship to cocrystals, inclusion compounds, and polymorphs. *Chem. Rev.* **2015**, *115*, 2895–2933.
- (22) Pettersson, K. Configurational studies in the α -phenyl carboxylic acid series: Hydratropic and α -phenylbutyric acid. *Ark. Kemi* **1956**, *10*, 283–296.

- (23) Lodochnikova, O. A.; Kosolapova, L. S.; Saifina, A. F.; Gubaidullin, A. T.; Fayzullin, R. R.; Khamatgalimov, A. R.; Litvinov, I. A.; Kurbangalieva, A. R. Structural aspects of partial solid solution formation: two crystalline modifications of a chiral derivative of 1,5-dihydro-2*H*-pyrrol-2-one under consideration. *CrystEngComm* **2017**, 19, 7277–7286.
- (24) Kitaigorodsky, A. I. *Mixed Crystals*; Springer-Verlag: Berlin, 1984.
- (25) Jacques, J.; Collet, A.; Wilen, S. H. Enantiomers, Racemates, and Resolutions; Krieger Publishing: Malabar, Florida, 1991.
- (26) Brandel, C.; Petit, S.; Cartigny, Y.; Coquerel, G. Structural aspects of solid solutions of enantiomers. *Curr. Pharm. Des.* **2016**, 22, 4929–4941.
- (27) Rekis, T.; Bērziņš, A.; Orola, L.; Holczbauer, T.; Actiņš, A.; Seidel-Morgenstern, A.; Lorenz, H. Single enantiomer's urge to crystallize in centrosymmetric space groups: Solid solutions of phenylpiracetam. *Cryst. Growth Des.* **2017**, *17*, 1411–1418.
- (28) Etter, M. C.; MacDonald, J. C.; Bernstein, J. Graph-set analysis of hydrogen-bond patterns in organic crystals. *Acta Crystallogr., Sect. B: Struct. Sci.* **1990**, *46*, 256–262.
- (29) Jeffrey, G. A. An Introduction to Hydrogen Bonding; Oxford University Press: New York and Oxford, 1997.
- (30) Phan, C. U.; Shen, J.; Yu, K.; Mao, J.; Tang, G. Impact of crystal habit on the dissolution rate and in vivo pharmacokinetics of sorafenib tosylate. *Molecules* **2021**, *26*, 3469.
- (31) Bukovec, P.; Benkic, P.; Smrkolj, M.; Vrecer, F. Effect of crystal habit on the dissolution behaviour of simvastatin crystals and its relationship to crystallization solvent properties. *Pharmazie* **2016**, *71*, 263–268.
- (32) Krivoshein, A. V.; Lindeman, S. V.; Bentum, S.; Averkiev, B. B.; Sena, V.; Timofeeva, T. V. Molecular arrangements in crystals of racemic and enantiopure forms of *N*-carbamoyl-2-phenylbutyramide and 2-phenylbutyramide: differences and similarities. *Z. Kristallogr.-Cryst. Mater.* **2018**, 233, 781–793.
- (33) Timofeeva, T. V.; Sena, V.; Averkiev, B. B.; Bejagam, S. N.; Usman, M.; Krivoshein, A. V. Unusual polymorphs of *rac*-3-phenylpyrrolidine-2,5-dione with $Z^\prime=1$, 2, and 3. *CrystEngComm* **2019**, 21, 6819–6829.
- (34) Ayala, A. P. Polymorphism in drugs investigated by low wavenumber Raman scattering. *Vib. Spectrosc.* **2007**, *45*, 112–116.
- (35) Roy, S.; Chamberlin, B.; Matzger, A. J. Polymorph discrimination using low wavenumber Raman spectroscopy. *Org. Process Res. Dev.* **2013**, *17*, 976–980.